PCCP

Accepted Manuscript

Journal Name

ARTICLE

Europium (II)-Activated Oxonitridosilicate Yellow Phosphor with Excellent Quantum Efficiency and Thermal Stability - A Robust Spectral Conversion Material for Highly Efficient and Reliable White LEDs

Le Wang,*[a] Hong Zhang,[a] Xiao-Jun Wang,[b] Benjamin Dierre,[b] Takayuki Suehiro,[b] Takahashi Takeda,[b] Naoto Hirosaki,[b] Rong-Jun Xie*[bc]

Clarifying physiochemical properties of a material is of great importance to design and utilize it in a right way. In this paper, we conduct a comprehensive survey of photoluminescence spectra, localized cathodoluminescence, temperature-dependent luminescence efficiency, and applications of Eu^{2+}-doped $Sr_{0.5}Ba_{0.5}Si_2O_2N_2$ in solid state lighting. This phosphor exhibits a broad emission band with a maximum at 560-580 nm and a full-width at half maximum of 92-103 nm upon the blue light excitation, whereas a dual-band emission (*i.e.,* 470 nm and 550 nm) is observed under the electron beam irradiation due perhaps to the intergrowth of $BaSi_2O_2N_2:Eu^{2+}$ and $Sr_{0.5+\sigma}Ba_{0.5-\sigma}Si_2O_2N_2:Eu^{2+}$ in each phosphor particle. Under the 450 nm blue light irradiation, this yellow phosphor exhibits excellent luminescence properties with absorption, internal and external efficiencies of 83.2, 87.7 and 72.6%, respectively. Furthermore, it also possesses high thermal stability, with the quantum efficiency being decreased by only 4.2% at 150°C and a high quenching temperature of 450°C. High efficiency white LEDs using the title phosphor have the luminous efficacy, color temperature and color rendition of ~120 lm/W, 6,000 K and 61 respectively, validating its suitability for use in solid state white lighting.

1. INTRODUCTION

White light-emitting diodes (wLEDs) are now penetrating into the lighting market rapidly, replacing traditional incandescent bubbles and fluorescent tubes for general lighting as well as cold cathode fluorescent lamps (CCFL) for liquid crystal display (LCD) backlights, because they promise energy-saving, high brightness, high reliability, long lifetime, and environmental friendly.[1-4] Phosphors (inorganic luminescent materials) are one of key materials in wLEDs, which down-convert the emission of LED chips into visible light, and thus play an important role in determining the efficiency, colour temperature, colour rendition and lifetime of wLED lamps.[5-8] The first wLED was fabricated by pumping a yellow-emitting yttrium aluminum garnet phosphor (YAG:Ce) with a blue InGaN LED chip, which is also called one-phosphor converted (1-pc) wLED.[4] The 1-pc wLEDs exhibit lower colour rendition than the multi-phosphor-converted ones, but have lower manufacturing cost and higher

luminous efficiency. They are therefore extensively used as flashlights, footlights, streetlights, outdoor lighting, headlamps, and so on.

In 1-pc wLEDs, a yellow-emitting phosphor is pumped by a blue LED chip, so that the phosphor is required to absorb blue light strongly and have high quantum efficiency. In short, the excitation spectrum of the yellow phosphor needs to match well with the emission spectrum of blue LEDs. Besides the popularly used YAG:Ce, a number of yellow-emitting phosphors have been investigated as potential spectral conversion luminescent materials, which include orthosilicates, phosphates, oxyfluorides, carbodiimide, and (oxy)nitrides.[9-28] For example, Park *et al.* reported Eu^{2+}-doped alkaline earth orthosilicates, $Sr_3SiO_5:Eu^{2+}$, which emits at ~ 570 nm and can produce white light with CCT = 4500 K and Ra = 64 when coupled to a blue LED.[9] Im *et al.* identified a blue-light-excitable yellow phosphor $LaSr_2AlO_5:Ce^{3+}$ (λ_{em} = 552-577 nm), and used it to fabricate white LEDs with CCT = 4300-5100 K and Ra = 80-82.[12] Xie *et al.* discovered orange-emitting Ca-α-sialon:Eu^{2+} (λ_{em} = 580-603 nm) and yellow-green-emitting Li-α-sialon:Eu^{2+} (λ_{em} = 560 -575 nm), the former was used to create warm white with correlated color temperature (CCT) of ~ 3,000 K, and the latter to produce white light with CCT of ~ 4500 K.[5, 7, 20, 21] Suehiro *et al.* reported a broadband yellow phosphor $La_3Si_6N_{11}:Ce^{3+}$ (λ_{em} = 577 -581 nm), which has an external quantum efficieicny of 42% under the 450 nm excitation.[24] Warm white with CCT = 2600-3800 K and Ra = 65-69 can be achieved by using $La_3Si_6N_{11}:Ce^{3+}$.[24] On the other hand, these

[a.] *College of Optics and Electronic Science and Technology, China Jiliang University, Hangzhou, Zhejiang 310018, China.Email: calla@cjlu.edu.cn*

[b.] *Sialon Group, Sialon Unit, Materials for Environment and Energy Division, National Institute for Materials Science (NIMS), Namiki 1-1, Tsukuba, Ibaraki 305-0044, Japan. Email: Xie.Rong-Jun@nims.go.jp*

[c.] *College of Materials, Xiamen University, No. 422 Siming-nan Road, Xiamen, Fujian 361005, China.*

† Footnotes relating to the title and/or authors should appear here.
Electronic Supplementary Information (ESI) available: [details of any supplementary information available should be included here]. See DOI: 10.1039/x0xx00000x

phosphors generally show lower absorption of blue light and conversion efficiency than YAG:Ce^{3+}, searching for highly efficient yellow phosphors is thus continuously pursued by materials scientists and chemists.
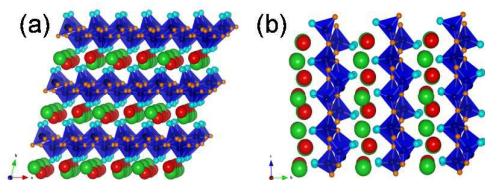
Figure 1 Crystal structure of Sr$_{0.5}$Ba$_{0.5}$Si$_2$O$_2$N$_2$ projected along the [100] (left) and along the [001] (right) directions (Sr$_I$/Ba$_I$ atoms: green, Sr$_{II}$/Ba$_{II}$ atoms: red, O atoms: cyan, and N atoms: orange).

Alkaline earth oxonitridosilicates, MSi$_2$O$_2$N$_2$:Eu^{2+} (M = Ca, Sr, Ba), have been shown interesting blue-green (BaSi$_2$O$_2$N$_2$:Eu^{2+}, λ$_{em}$ = 495 nm), green (SrSi$_2$O$_2$N$_2$:Eu^{2+}, λ$_{em}$ = 540 nm) and yellow (CaSi$_2$O$_2$N$_2$:Eu^{2+}, λ$_{em}$ = 555 nm) emissions, exhibiting a broadband excitation spectrum covering the blue spectral region.[29-32] The emission colour of these phosphors is tunable by forming solid solutions between the end members. Partial substitution of Sr^{2+} by Ca^{2+} or Ba^{2+} leads to a redshift of the Eu^{2+} emission, due to the increased crystal-field splitting (Ca^{2+}→ Sr^{2+}) or a less restricted local lattice relaxation at the Eu^{2+} sites (Ba^{2+}→ Sr^{2+}).[25, 30, 31,32] Li *et al.* addressed three different crystal structures or phases depending on the degree of the Ba substitution for Sr, and emphasized the crucial role of the localized structure in tailoring the luminescence properties.[32] An interesting yellow-emitting phosphor is therefore attained in the composition of Sr$_{0.5}$Ba$_{0.5}$Si$_2$O$_2$N$_2$:Eu^{2+}.[25, 30, 31, 32] Schnick *et al.* revealed the real structure of Sr$_{0.5}$Ba$_{0.5}$Si$_2$O$_2$N$_2$, which is isotypic to SrSi$_2$O$_2$N$_2$ with a twinned layered oxonitridosilicate with disordered metal atoms (see Fig. 1).[25] It crystallizes in a triclinic system with space group of P1, and lattice parameters are a = 7.2059(2), b = 7.3887(3), c = 7.3340(2) Å, α = 88.524(4), β = 84.454(3), γ = 75.980(4). There are two Sr/Ba crystallographic sites, and each Sr/Ba atom is coordinated to six oxygen atoms and one nitrogen atom. The average bond length of Sr-O is 2.68 Å. They also discussed the relations between the crystal structure and the luminescence of Sr$_{0.5}$Ba$_{0.5}$Si$_2$O$_2$N$_2$:Eu (2 mol% Eu), and clarified the abnormal redshift of the Eu^{2+} emission with the Ba substitution.[25]

As a potential yellow luminescent material for solid state lighting, a deeper insight into the photoluminescence properties is extremely important and required to optimize its performance in a device. In this work, comprehensive investigations on the title phosphor were carried out to understand the optimal concentration, absorption and quantum efficiency, temperature-dependent luminescence efficiency, localized luminescence and microstructure. The suitability of the phosphor in solid state lighting was also testified by combining it to a blue LED chip, and the optical properties of the device were presented.

2. MATERIALS AND EXPERIMENTAL DETAILS

2.1. Synthesis

Phosphor samples, with compositions of Sr$_{0.5-x}$Eu$_x$Ba$_{0.5}$Si$_2$O$_2$N$_2$ (x = 0.005-0.12), were prepared by a two-step firing method mentioned in the literature.[30] Firstly, the (Sr$_{0.5}$Ba$_{0.5}$)$_2$SiO$_4$:Eu^{2+} precursor powder was prepared by firing the powder mixture of SrCO$_3$, BaCO$_3$, Eu$_2$O$_3$

and SiO$_2$ at 1500°C for 6 h in a tube furnace filled with the flowing N$_2$-H$_2$ (95%/5%) mixture gas. Then, the (Sr$_{0.5}$Ba$_{0.5}$)$_2$SiO$_4$:Eu^{2+} powders were pulverized, sieved, and mixed with an appropriate amount of α-Si$_3$N$_4$. This powder mixture was again fired at 1650°C for 6 h. The phosphor powder was finally obtained by grinding, sieving and washing in dilute HCl and deionized water.

2.2. Photoluminescence spectra, Quantum Efficiency and Decay Time

Photoluminescence spectra were measured at room temperature using a fluorescent spectrophotometer (F-4500, Hitachi Ltd., Japan) with a 200 W Xe-lamp as an excitation source. The emission spectrum was corrected for the spectral response of a monochromater and Hamamatsu R928P photomultiplier tube by a light diffuser and tungsten lamp (Noma, 10V, 4A). The excitation spectrum was also corrected for the spectral distribution of the xenon lamp intensity by measuring Rhodamine-B as reference. External (η$_0$) and internal (η$_i$) quantum efficiencies (QEs) were calculated by using the following equations:[33]

$$\eta_0 = \frac{\int \lambda \bullet P(\lambda)d\lambda}{\int \lambda \bullet E(\lambda)d\lambda}$$
$$\eta_i = \frac{\int \lambda \bullet P(\lambda)d\lambda}{\int \lambda \{E(\lambda)- R(\lambda)\}d\lambda} \qquad (1)$$

where E(λ)/hν, R(λ)/hν and P(λ)/hν are the number of photons in the spectrum of excitation, reflectance and emission of the phosphor, respectively. The luminescence spectra for QE measurement were recorded by an intensified multichannel spectrometer (MCPD-7000, Otsuka Electronics, Japan). The reflection spectrum of spectralon diffusive white standards was used for calibration. Fluorescence lifetime data were collected by using a time-correlated single-photon counting fluorometer (TemPro, Horiba Jobin-Yvon) equipped with a NanoLED-370 nm with the pulse duration full width at half-maximum of ∼1ns.

2.3. Cathodoluminescence

Scanning electron microscopy (SEM) and cathodoluminescence (CL) measurements were executed by a field emission SEM (Hitachi, S4300) equipped with a CL system (Horiba, MP32S/M). The beam current was fixed at 100 pA and the e-beam energy at 5 kV, which corresponds to a penetration depth of ~350 nm, according to the Kanaya–Okayama model.[34] All the measurements were done at room temperature.

2.4. Temperature-Dependent Luminescence and Efficiency

The temperature-dependent luminescence (thermal quenching) was measured by an intensified multichannel spectrometer (MCPD-7000, Otsuka Electronics, Japan). The phosphor powders were heated up to 250°C in 25°C intervals at a heating rate of 100°C/min, and held at each temperature for 5 min. The temperature-dependent quantum efficiency was evaluated by using a QE-1100 phosphor quantum yield spectrophotometer (Otsuka Electronics, Japan).

2.5. Microstructure characterizations

Microstructure observations and energy-dispersed x-ray spectroscopy (EDS) measurements of the phosphor samples were carried out at room temperature using a high-resolution field emission scanning electron microscope (Hitachi, S4800).

3. RESULTS AND DISCUSSION

3.1 Photoluminescence Spectra

As seen in Fig. 2, the excitation spectrum of $Sr_{0.5-x}Eu_xBa_{0.5}Si_2O_2N_2$ is quite broad, covering the spectral range of 250 to 500 nm. This broad excitation band can be deconvoluted into five sub-bands by Gaussian fitting, which are centered at 260, 304, 350, 406, and 472 nm, respectively. These sub-bands can be considered as five 5d energy levels of Eu^{2+}, so that the crystal field splitting and the center of gravity are then calculated as 17,200 and 36,400 cm^{-1} respectively. The emission spectrum exhibits an unsymmetrical band with the maximum at 570 nm (x = 0.04), and the full width at half maximum (FWHM) is about 94 nm. The Stoke shift is thus roughly estimated as 3,600 cm^{-1}, which is quite close to 3,573 cm^{-1} reported in the literature.[25] The larger Stokes shift observed in the Ba-substituted $SrSi_2O_2N_2$ contributes to the redshifted emission of $SrSi_2O_2N_2$:Eu^{2+} (568 nm *vs* 540 nm), which can be interpreted by a less restricted local lattice relaxation at the Eu^{2+} sites.[25]
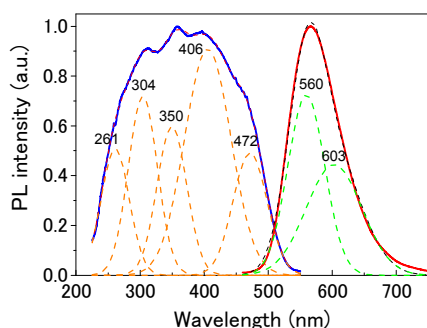
Figure 2 Excitation (left) and emission (right) spectra of $Sr_{0.5-x}Eu_xBa_{0.5}Si_2O_2N_2$ (x = 0.04). The emission spectrum was measured under the 450 nm irradiation, and the excitation spectrum was monitored at 570 nm.
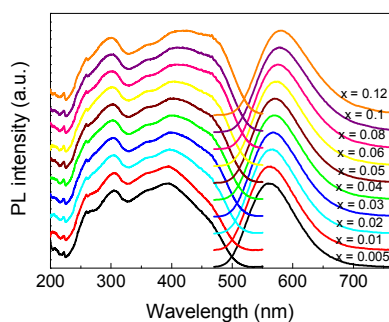
Figure 3 Excitation and emission spectra of $Sr_{0.5-x}Eu_xBa_{0.5}Si_2O_2N_2$ with varying Eu concentrations.
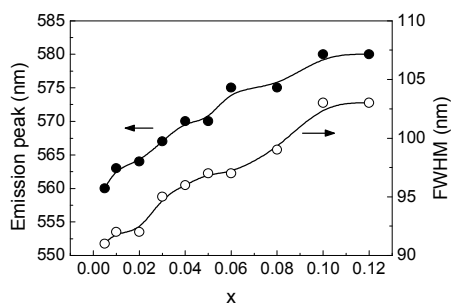
Figure 4 Variations of the emission peak and the full width at half maximum (FWHM) of $Sr_{0.5-x}Eu_xBa_{0.5}Si_2O_2N_2$ as a function of the Eu concentration (x).

With increasing the Eu concentration, both of the excitation and emission bands are red-shifted, as shown in Fig. 3. The emission maximum is linearly increased, shifting from 560 to 580 nm when the Eu concentration increases from x = 0.005 to x = 0.15, as shown in Fig. 4. At the same time, the emission band broadens with increasing the doping level, resulting in the increase of FWHM (Fig. 4). The right wing of the excitation spectrum is intensified gradually as the Eu doping level increases. These increases are mainly ascribed to the enhanced covalence of the Eu-O band with respect to the Sr-O band due to the larger Paulling electronegativity of Eu (Sr: 0.95, Eu: 1.2, O: 3.44).[35]
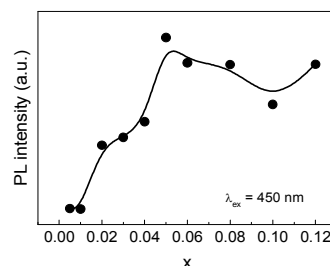
Figure 5 Effect of the Eu concentration on the emission intensity of $Sr_{0.5-x}Eu_xBa_{0.5}Si_2O_2N_2$. The samples were excited at 450 nm.

The concentration quenching occurs when the Eu concentration reaches x = 0.05, as shown in Fig. 5. The concentration quenching is dominantly ascribed to the energy transfer between Eu^{2+}. The critical distance (R_c) for the energy transfer can be estimated by using the formula suggested by Blasse:[36]

$$R_c \approx 2\left[\frac{3V}{4\pi x_c N}\right]^{1/3} \qquad (2)$$

Here x_c is the critical concentration, N the number of cation sites in the unit cell, and V the volume of the unit cell. For $Sr_{0.5}Ba_{0.5}Si_2O_2N_2$, x_c = 0.05, N = 4, and V = 377.07 $Å^3$. By using the equation, the critical distance for energy transfer is calculated to be 15.33 Å. The decay time for $Sr_{0.5-x}Ba_{0.5}Si_2O_2N_2$:$Eu_x$ is 0.95 - 1.07 μs, which is in the range of decay time usually for Eu^{2+} (*i.e.*, 0.2 – 2 μs).[37, 38] A tendency in the reduction of decay time with increasing the dopant concentration is seen in Fig.6, although the decline is quite small. Taking into account of the experimental error, it is noted that the decay time nearly keeps invariable when the Eu concentration reaches x ~ 0.5. The variation in decay time is consistent with the concentration quenching shown in Fig.5.

As we may know, the excited Eu^{2+} centres can decay to the ground state by radiative and nonradiative processes, giving a so-called decay time signal. The total decay rate A_T is the sum of the radiative (A_0) and nonradiative (A_{nr}) rates, which can also be written as

$$A_T = A_0 + A_{nr} \qquad (3)$$

Or

$$\frac{1}{\tau} = \frac{1}{\tau_0} + \frac{1}{\tau_{nr}} \qquad (4)$$

Where τ, τ_0 and τ_{nr} is the luminescence decay time, radiative and nonradiative decay time, respectively. Given that the nonradiative decay time of a very diluted sample is zero, the radiative decay time of $Sr_{0.5}Ba_{0.5}Si_2O_2N_2$:Eu can be obtained from the sample with x =

0.005, i.e., τ_0 = 1.072 μs. Therefore, the decrease of the luminescence decay time with increasing the Eu concentration definitely leads to the enhanced nonradiative rate (Fig. 6), indicative of the luminescence loss caused by the radiativeless energy transfer.
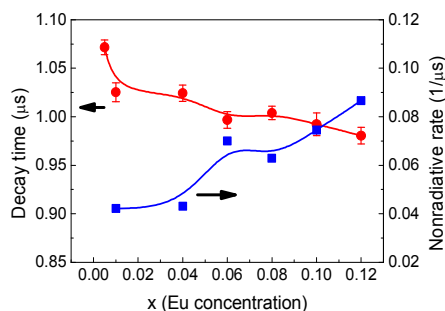
Figure 6 Decay time of $Sr_{0.5-x}Eu_xBa_{0.5}Si_2O_2N_2$ as a function of the Eu concentration. The samples were excited at 370 nm and the 568 nm emission was monitored.

3.2. Dual-Band Cathodoluminescence

Differing from photoluminescence that only excites electrons into energy levels with energies lower than incident photons, cathodoluminescence promises to pump the electrons directly into the conduction band of host crystals, thus enabling to detect the emissions that cannot be appreciably found in the PL measurement, and allowing to understanding the localized luminescence of phosphors. A great difference between photoluminescence spectrum and cathodoluminescence one is clearly seen in Fig. 7, where the CL spectrum of one phosphor particle exhibits two emission bands centred at 470 and 550 nm, respectively. These two bands cannot be assigned to the emissions from two different crystallographic sites of Eu (Sr/Ba), because both Eu atoms are bonded to six oxygen atoms and one nitrogen atom at similar distances.
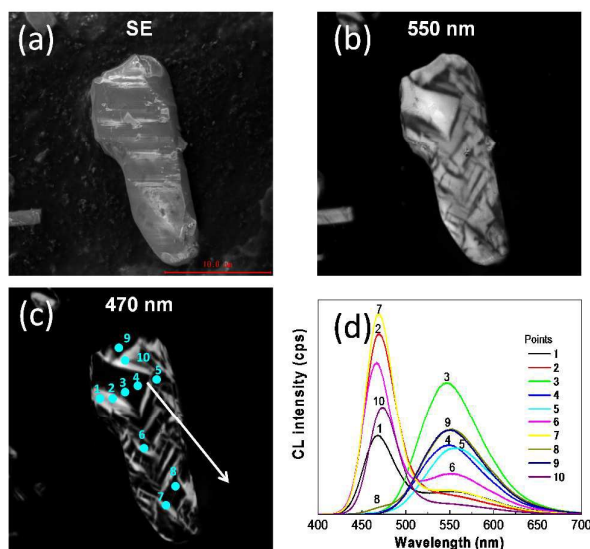
Figure 7 (a) SEM image of a single phosphor particle, and CL mapping of (b) 550 nm emission, (c) 470 nm emission, and (d) position-dependent CL spectra of the phosphor particle.

To understand the origin of these two bands, the local CL monochromatic images were used. The spatial distribution of blue and yellow band emissions is given by the CL intensity images, which can be considered as a CL intensity map of luminescence excited by the scanned electron beam at the selected emission wavelength. As seen, there are two separate emitting areas with distinct colours even in one phosphor particle, indicating that the blue and yellow emissions are originated from two different phases rather than one phase with two luminescence centers. This is also evidenced by the great difference in the band width of the emission spectra. The full width at half maximum of the emission band is 37 and 82 nm for 470 and 550 nm, respectively. The very narrow emission band centered at 470 nm is equivalent to that of $BaSi_2O_2N_2:Eu^{2+}$ that has a different crystal structure from $Sr_{0.5}Ba_{0.5}Si_2O_2N_2$.[29, 31] It is thus supposed that the intergrowth of $Sr_{0.5+\sigma}Ba_{0.5-\sigma}Si_2O_2N_2$ (it has a shorter emission wavelength than $Sr_{0.5}Ba_{0.5}Si_2O_2N_2$, so $\sigma \neq 0$) and $BaSi_2O_2N_2$ occurs in each particle, forming an interesting and special woven structure. As seen in Fig.8, the elemental mapping of Si, O, N and Eu is very uniform in a phosphor particle investigated, whereas that of Sr and Ba is obviously position-dependent. It evidences the intergrowth of a Ba-enriched phase ($BaSi_2O_2N_2$) and a Sr/Ba-contained phase ($Sr_{0.5+\sigma}Ba_{0.5-\sigma}Si_2O_2N_2$). Schnick et al. [25] addressed that crystallites of $Sr_{0.5}Ba_{0.5}Si_2O_2N_2:Eu^{2+}$ were built up of small anti-phase domains within larger twin domains, and Li et al.[32] also confirmed the nanophase segregation and mixing in some compositions. Both observations support the proposed intergrowth in this work. The discussion of the intergrowth structure is beyond the scope of this work, and will be presented elsewhere.
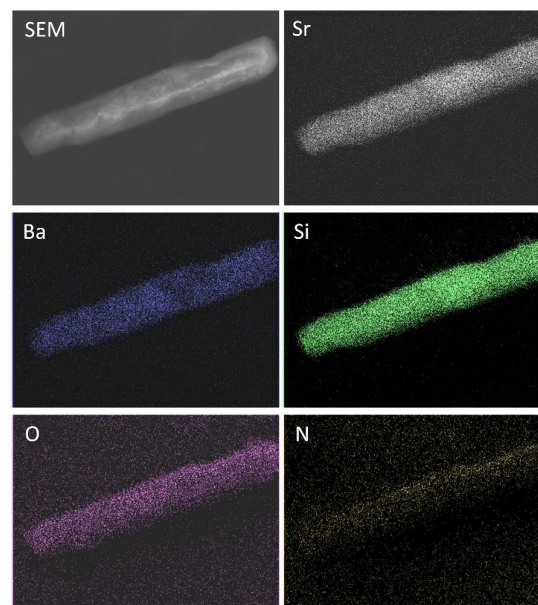
Figure 8 EDS elemental mapping of $Sr_{0.5-x}Eu_xBa_{0.5}Si_2O_2N_2$ (x = 0.04).

The dual-band cathodoluminescence is not solely limited to one or several particle(s) but a universal phenomenon for the title phosphor. On the other hand, such a dual-band emission is not observed in samples under the 450 nm blue light irradiation, which can be attributed to reabsorption as a result of the broadband

excitation spectrum covering the UV-to-blue spectral region. Therefore, the dual-band cathodoluminescence will not affect the title phosphor to be used as a LED phosphor. In addition, Li *et al.* observed a similar dual-band emission for phosphors with y > 0.65 in $Sr_{1-y}Ba_ySi_2O_2N_2$:Eu when excited at 405 nm, so that the color tuning could be realized by just controlling the Sr/Ba ratio.[32]
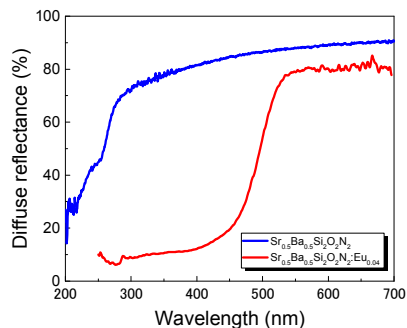
Figure 9 Diffuse reflectance spectra of $Sr_{0.5}Ba_{0.5}Si_2O_2N_2$ and $Sr_{0.5-x}Eu_xBa_{0.5}Si_2O_2N_2$ (x = 0.04).
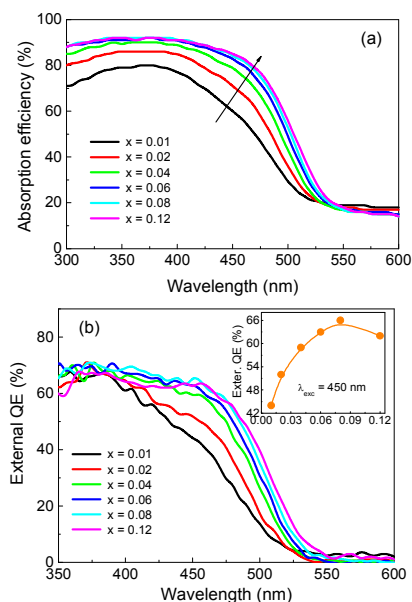
Figure 10 (a) Absorption spectra and (b) external quantum efficiency of $Sr_{0.5-x}Eu_xBa_{0.5}Si_2O_2N_2$ with varying Eu concentrations.

3.3. Diffuse Reflectance, Absorption and Quantum efficiency

The diffuse reflectance spectra of samples of x = 0 and 0.04 are given in Fig. 9. The optical absorption edge of the $Sr_{0.5}Ba_{0.5}Si_2O_2N_2$ host is situated at ~213 nm, indicative of the band gap of 5.82 eV which is a little bit larger than 5.6 eV for $SrSi_2O_2N_2$.[39] The onset of the optical absorption edge of the phosphor is located at 444.5 nm (~2.79 eV), which is ascribed to the 4f → 5d electronic transition of Eu^{2+}. As the doping amount of Eu increases, the absorption band is clearly seen to redshift (see Fig. 10a). The redshift is in a good agreement with the changes in excitation spectrum with the dopant concentration. Meanwhile, the absorption of the phosphor is enhanced with increasing the Eu content. Upon the 450 nm excitation, the absorption efficiency increases obviously from 60 to

85% for x = 0.01 and 0.12, respectively. For phosphors in solid state lighting, the blue light absorption is required to be as high as possible, enabling more photons to be involved in the luminescence process.

The effect of the Eu concentration on the external quantum efficiency of the yellow phosphors is shown in Fig. 10b. Upon the blue light irradiation, the efficiency is optimized at x = 0.08 (66%). It is not consistent with the critical concentration for concentration quenching (*i.e.*, x = 0.05). The reason for this difference can be explained by the different variations of absorption efficiency and internal quantum efficiency with the Eu concentration. As we may know, quantum efficiency, including internal and external quantum ones, is a key parameter for understanding the luminescence efficiency of a phosphor. The internal quantum efficiency is the ratio of the number of photons emitted by the sample to the number of photons absorbed by the sample, whereas the external one is the ratio of the number of photons emitted by the sample to the number of incident photons to the sample. Therefore, the external quantum efficiency is equal to the internal one multiplied by the absorption efficiency, which is thus usually smaller than the internal one. This loss is ascribed to the nonradiative photophysical processes such as scattering, trapping or energy transfer. The internal quantum efficiency is proportional to the integrated emission spectra that has the maximum at x = 0.05, which is also in agreement with concentration quenching (or decay time), whereas the absorption efficiency continuously increases with increasing the Eu concentration. This finally results in an optimized dopant concentration (*i.e.*, x = 0.08) for the external quantum efficiency that is different from the one for internal quantum efficiency.

3.4. Temperature-Dependent Luminescence Efficiency

Thermal stability is one of key technological parameters for phosphors used in solid state lighting because the GaN-based chip generates heat that will quench the luminescence of spectral conversion materials. It can be evaluated by measuring the temperature dependent luminescence efficiency including photoluminescence intensity and quantum efficiency. As shown in Fig. 11, the photoluminescence intensity tends to decline as the temperature rises, due to the thermally-induced non-radiative energy transfer. The photoluminescence intensity at 150 and 200°C maintains 90 and 84% of the initial intensity (25°C) respectively, indicative of very small thermal quenching and of good thermal stability of $Sr_{0.5}Ba_{0.5}Si_2O_2N_2$:$Eu^{2+}$. The thermal quenching temperature ($T_{50\%}$) is about 450°C, which is much higher than 288°C (*i.e.*, 560K) reported by Bachmann.[31] This difference is ascribed to the variations in firing temperature, the higher temperature (1650°C vs 1500°C) used at this work results in a pure phase with less orthosilicate impurities.[25] The activation energy for thermal quenching is calculated as 0.161 ± 0.005 eV for $Sr_{0.46}Ba_{0.5}Si_2O_2N_2$:$Eu_{0.04}$ (x = 0.04). Moreover, with increasing temperature the emission spectrum is blueshifted slightly, with the left wing enhanced. This is ascribed to the increased probability of radiative transitions from higher energy levels of the 5d electron orbitals of Eu^{2+}. In addition, the thermal quenching temperature decreases a little with increasing the Eu^{2+} concentration.

The temperature dependent quantum efficiency of $Sr_{0.46}Ba_{0.5}Si_2O_2N_2$:$Eu_{0.04}$ was measured for the first time, as shown in

Fig. 12. Under the 450 nm excitation, both internal and external quantum efficiency slightly decreases with increasing temperature, reduced by 4.1 and 2.6% at 150°C respectively. The reduction is much less than that in the peak emission intensity (by 10% at 150°C). The small temperature-dependent luminescence and quantum efficiency imply that $Sr_{0.5}Ba_{0.5}Si_2O_2N_2$:$Eu^{2+}$ is a thermally stable yellow phosphor.
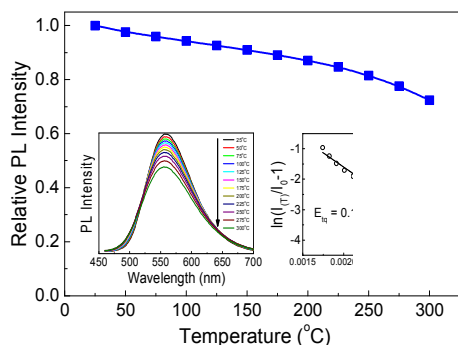
Figure 11 Thermal quenching of $Sr_{0.5-x}Eu_xBa_{0.5}Si_2O_2N_2$ (x = 0.04). The samples were excited at 450 nm.
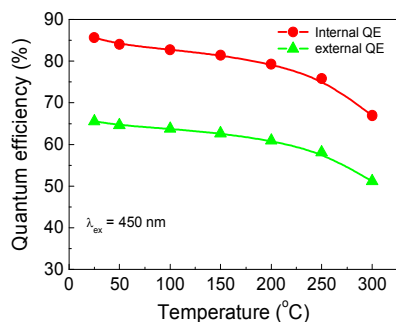
Figure 12 Temperature-dependent quantum efficiency of $Sr_{0.5-x}Eu_xBa_{0.5}Si_2O_2N_2$ (x = 0.04). The samples were excited at 450 nm.

3.5. Luminescence Efficiency Enhanced by Post-Treatment

In most cases, phosphors are usually post-treated for achieving higher efficiency and tailoring the particle size as well as particle size distribution. The sample of x = 0.04 was selected for post-treatments such as a dilute HCl acid washing. It is clearly seen that the treated sample has coarsened and smoothed particles, of which the average particle size (D_{50}) is around 24.7 μm (vs 27.7 μm for the untreated sample) and the degree of dispersion (S) is 1.46 (vs 1.82) (Fig. 13). These enhancements are ascribed to the removal of tiny particles as well as residual impurities associated with the acid cleaning.

The acid cleaning also leads to the improvements in luminescence efficiency, as shown in Fig. 14. Upon the 450 nm excitation, the absorption, internal and external efficiencies of the treated sample are 83.2, 87.7 and 72.6%, increased by 6.4, 5.6 and 10% respectively. Less scattering and surface defects are considered to account for the enhanced efficiency of the treated phosphor. In addition, the post-treatment does not alter the thermal quenching behaviour of the sample. As shown in Table 1, except for the well-known YAG:Ce the $Sr_{0.5}Ba_{0.5}Si_2O_2N_2$:Eu phosphor exhibits higher luminescence efficiency and smaller thermal quenching compared

to other promising yellow nitride or orthosilicate phosphors, enabling it to be an excellent colour converter for white LEDs with high luminous efficiency.
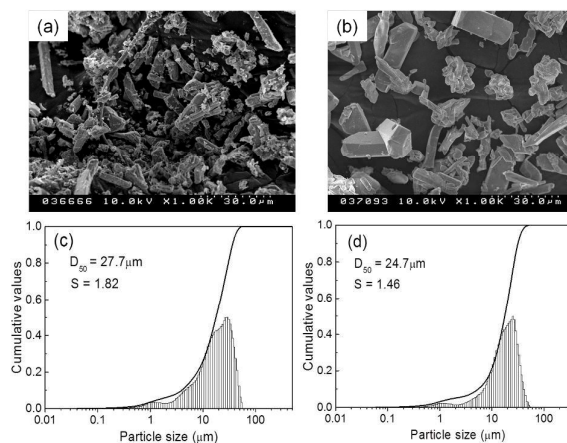
F**igure 13** SEM images of (a) as-prepared and (b) acid cleaned, and particle size distributions of (c) as-prepared and (d) acid cleaned $Sr_{0.5-x}Eu_xBa_{0.5}Si_2O_2N_2$ (x = 0.04).
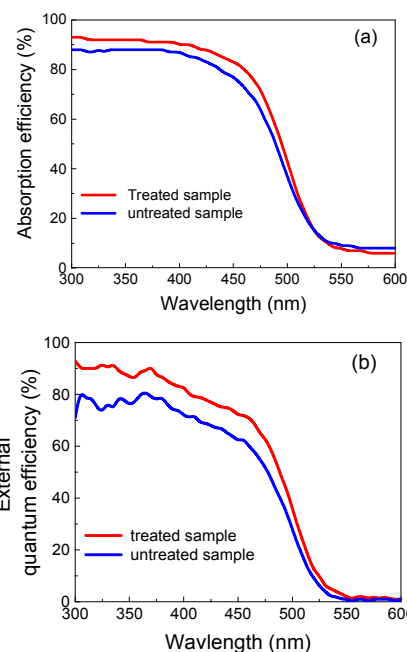
Figure 14 (a) Absorption, (b) external quantum efficiency of $Sr_{0.5-x}Eu_xBa_{0.5}Si_2O_2N_2$ (x = 0.04) before and after the acid cleaning.

Table I Photoluminescence properties of several yellow phosphors for solid state lighting (E.Q.E and T.Q. is the external quantum efficiency and thermal quenching, respectively)

Phosphors	λ_{max} /nm	FWHM /nm	E.Q.E /%	T.Q. /%	Ref.
$Y_3Al_5O_{12}$:Ce^{3+}	555	122	81	87	5
$La_3Si_6N_{11}$:Ce^{3+}	580	120	60	84	24
$Sr_2Ba(AlO_4F)_{1-x}(SiO_5)_x$:$Ce^{3+}$	539	125	63	82	15
$CaAlSiN_3$:Ce^{3+}	580	135	54	87	22
$(SrBa)_2SiO_4$:Eu^{2+}	552	92	63	85	9
Ca-α-sialon:Eu^{2+}	585	94	59	90	5
$Sr_{0.5}Ba_{0.5}Si_2O_2N_2$:$Eu^{2+}$	560	93	72	90	This work

3.6. Applications in White LEDs

The suitability of the $Sr_{0.5}Ba_{0.5}Si_2O_2N_2$:Eu yellow phosphor in white LEDs was also testified in this work. White LED lamps were fabricated by mounting a blend mixture of about 0.1500 g phosphor powders and 2.3916 g silicone resin on a blue LED chip (λ_{em} = 450 nm). Figure 15 shows the electroluminescence spectrum of a white LED driven at a 20 mA current. The lamp has a correlated color temperature (CCT) of 5970 K, colour rendering index (Ra) of 61, and CIE chromatic coordinates (x, y) of (0.323, 0.328). The luminous efficacy of the white LED is as high as 117 lm/W. These results demonstrate that $Sr_{0.5}Ba_{0.5}Si_2O_2N_2$:Eu has strong potential applications in developing highly efficient, thermally stable cool white LEDs.
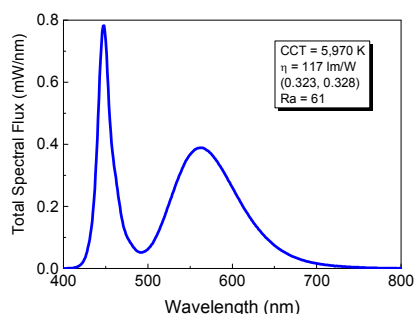
Figure 15 Electroluminescence spectrum of white LEDs prepared by combining $Sr_{0.5-x}Eu_xBa_{0.5}Si_2O_2N_2$ (x = 0.04) with a blue LED chip, measured under a 20 mA drive current at room temperature.

4. CONCLUSIONS

Knowing of the detailed physiochemical properties of a material is of great importance for properties optimization and practical applications. In this work, a throughout investigation has been carried out to elucidate photoluminescence properties and the temperature-dependent luminescence efficiency of a yellow-emitting $Sr_{0.5}Ba_{0.5}Si_2O_2N_2$:$Eu^{2+}$ phosphor for solid state lighting. This oxonitridosilicate phosphor shows high absorption and quantum efficiency of 83 and 88% upon the 450 nm excitation, respectively. It also possesses excellent thermal stability, with the thermal quenching temperature as high as 450°C. The woven structure observed by the CL mapping does not affect the photoluminescence properties, although it remains unclarified how it forms. White light LEDs with the luminous efficacy of ~120 lm/W and the colour temperature of ~ 6,000 K can be fabricated by combining this yellow phosphor with a blue LED chip (λ_{em} = 450 nm), indicative of a promising robust yellow colour converter for high efficiency and high reliability solid state lighting.

Acknowledgements

Notes and references

1   E.F. Schubert and J.K. Kim, *Science,* 2005, **308**, 1274-1278.

2   S. Nakamura, T. Mukai and M. Senoh, *Appl. Phys. Lett.,* 1994, **64**, 1687-1689.

3   S. Pimputkar, J.S. Speck, S.P. DenBaars and S. Nakamura, *Nature Photon.,* 2009, **3**, 180-182.

4   G. Fasol and S. Nakamura, *The Blue Laser Diode: GaN Based Blue Light Emitters and Lasers*; Springer: Berlin, 1997.

5   R.-J. Xie, Y.Q. Li, N. Hirosaki and H. Yamamoto, *Nitride Phosphors and Solid State Lighting*; CRC Press: Boca Raton, 2011.

6   C. Che and R.-S. Liu, *J. Phys. Chem. Lett.,* 2011, **2**, 1268-1277.

7   R.-J. Xie and N. Hirosaki, *Sci. Technol. Adv. Mater.,* 2007, **8**, 588-600.

8   S. Ye, F. Xiao, Y.X. Pan, Y.Y. Ma and Q.Y. Zhang, *Mater. Sci. Eng. R,* 2010, **71**, 1-34.

9   J.K. Park, C.H. Kim, S.H. Park, H.D. Park and S.Y. Choi, *Appl. Phys. Lett.,* 2004, **84**, 1647-1649.

10   H.S. Jang and D.Y. Jeon, *Appl. Phys. Lett.,* 2007, **90**, 041906-1-041906-3.

11   A. A. Setlur, W.J. Heward, Y. Gao, A.M. Srivastava, R.G. Chandran and M.V. Shankar, *Chem. Mater*., 2006, **18**, 3314-3322.

12   W.B.Im, N.N. Fellows, S.P. DenBaars, R. Seshadri and Y.-I1. Kim, *Chem. Mater.,* 2009, **21**, 2957-2966.

13   H.S. Jang, H.Y. Kim, Y.S. Kim, H.M. Lee and D.Y. Jeon, *Opt. Exp.,* 2012, **20**, 2761-2771.

14   C.H. Huang and T.M. Chen, *Inorg. Chem.,* 2011, **50**, 5725-5730.

15   K.A. Denault, N.C. George, S.R. Pade, S. Brinkley, A.A. Mikhailovsky, J.N. Neuefeind, S.P. DenBaars and R. Sashadri, *J. Mater. Chem.,* 2012, **22**, 18204-18213.

16   M. Krings, G. Montana, R. Dronskowski and C. Wickleder, *Chem. Mater.,* 2011, **23**, 1694-1699.

17   R.-J. Xie, M. Mitomo, K. Uheda, F.F. Xu and Y. Akimune, *J. Am. Ceram. Soc*., 2002, **85**, 1229-1234.

18   R.-J. Xie, N. Hirosaki, K. Sakuma, Y. Yamamoto and M. Mitomo, *Appl. Phys. Lett.,* 2004, **84**, 5404-5406.

19   R.-J. Xie, N. Hirosaki, M. Mitomo, Y. Yamamoto, T. Suehiro and K. Sakuma, *J. Phys. Chem. B,* 2004, **108**, 12027-12031.

20   R.-J. Xie, N. Hirosaki, M. Mitomo, K. Takahashi and K. Sakuma, *Appl. Phys. Lett*., 2006, **88**, 101104-1-101104-3.

21   R.-J. Xie, N. Hirosaki, M. Mitomo, K. Sakuma and N. Kimura, *Appl. Phys. Lett.,* 2006, **89**, 241103-1-241103-3.

22   Y.Q. Li, N. Hirosaki, R.-J. Xie, T. Takeda, and M. Mitomo, *Chem. Mater.,* 2008, **20**, 6704-6714.

23   T. Suehiro, H. Onuma, N. Hirosaki, R.-J. Xie, T. Sato and A. Miyamoto, *J. Phys. Chem. C,* 2010, **114**, 1337-1342.

24   T. Suehiro, N. Hirosaki and R.-J. Xie, *ACS Appl. Mater. Interfaces*, 2011, **3**, 811-816.

25   M. Seibald, O. Oeckler, V.R. Celinski, P.J. Schmidt, A. Tücks and W. Schnick, *Solid State Sci.,* 2011,**13**, 1769-1778.

26   W.B. Park, N. Shin, K.-P. Hong, M. Pyo and K.-S. Sohn, *Adv. Funct. Mater*., 2012, **22**, 2258-2266.

27   W.B. Park, Y.S. Jeong, S.P. Singh and K.-S. Sohn, *ECS J. Solid State Sci. Technol.,* 2013, **2**, R3100-R3106.

28   J. Ruan, R.-J. Xie, S. Funahashi, Y. Tanaka, T. Takeda, T. Suehiro, N. Hirosaki and Y.Q. Li, *J. Solid State Chem.,* 2013, **208**, 50-57.

29   Y.Q. Li, A.C.A. Delsing, G. de With and H.T. Hintzen, *Chem. Mater.,* 2005, **17**, 3242-3248.

30 B.G. Yun, Y. Miyamoto and H. Yamamoto, *J. Electrochem. Soc.*, 2007, **154**, J320-J325.

31 V. Bachmann, C. Ronda, O. Oeckler, W. Schnick and A. Meijerink, *Chem. Mater.,* 2009, **21**, 316-325.

32 G.Li, C.C. Lin, W.T. Chen, M.S. Molokeev, V.V. Atuchin, C.Y. Chiang, W. Zhou, C.W. Wang, W.H. Li, H.S. Sheu, T.S. Chan, C. Ma, and R.-S. Li, *Chem. Mater.*, 2014, **26**, 2991-3001.

33 K. Ohkubo and T. Shigeta, *J. Illum. Eng. Inst. Japan,* 1999, **83**, 87–93.

34 K. Kanaya and S. Okayama, *J. Phys. D: Appl. Phys.,* 1972, **5**, 43-58.

35 C. Housecroft and A.G. Sharpe, Inorganic Chemistry (3rd Edition). Prentice Hall: 2007.

36 G. Blasse, W.L. Wanmaker, J.W. TerVruggt and A. Bril, *Philips Res. Rep.,* 1968, **23**, 189-200.

37 J.L. Sommerdijk, J.M. Verstegen and A. Bril, *J. Lumin.,* 1974, **8**, 502-506.

38 R.F. Sosa, E.R. Alvarez, M.A. Comacho, A.F. Munoz and J.O. Rubio, *J. Phys.: Condens. Matter,* 1995, **7**, 6561-6568.

39 V. Bachmann,T. Justel, A. Meijerink, C. Ronda and P.J. Schmidt, *J. Lumin.*, 2006, **121**, 441-449.